IOP Publishing | Institute of Physics and Engineering in Medicine Physics in Medicine & Biology

Phys. Med. Biol. **62** (2017) 3263–3283 https://doi.org/10.1088/1361-6560/aa63d0

Computational hybrid anthropometric paediatric phantom library for internal radiation dosimetry

Tianwu Xie[1], Niels Kuster[2,3] and Habib Zaidi[1,4,5,6]

[1] Division of Nuclear Medicine and Molecular Imaging, Geneva University Hospital, 1211 Geneva 4, Switzerland
[2] Foundation for Research on Information Technologies in Society (IT'IS), Zeughausstr. 43, 8004 Zurich, Switzerland
[3] Swiss Federal Institute of Technology (ETH) Zurich, 8092 Zurich, Switzerland
[4] Geneva Neuroscience Center, Geneva University, 1205 Geneva, Switzerland
[5] Department of Nuclear Medicine and Molecular Imaging, University of Groningen, University Medical Center Groningen, 9700 RB Groningen, Netherlands
[6] Department of Nuclear Medicine, University of Southern Denmark, 500 Odense, Denmark

E-mail: habib.zaidi@hcuge.ch

Received 12 October 2016, revised 15 February 2017
Accepted for publication 1 March 2017
Published 28 March 2017

Abstract

Hybrid computational phantoms combine voxel-based and simplified equation-based modelling approaches to provide unique advantages and more realism for the construction of anthropomorphic models. In this work, a methodology and C++ code are developed to generate hybrid computational phantoms covering statistical distributions of body morphometry in the paediatric population. The paediatric phantoms of the Virtual Population Series (IT'IS Foundation, Switzerland) were modified to match target anthropometric parameters, including body mass, body length, standing height and sitting height/stature ratio, determined from reference databases of the National Centre for Health Statistics and the National Health and Nutrition Examination Survey. The phantoms were selected as representative anchor phantoms for the newborn, 1, 2, 5, 10 and 15 years-old children, and were subsequently remodelled to create 1100 female and male phantoms with 10th, 25th, 50th, 75th and 90th body morphometries. Evaluation was performed qualitatively using 3D visualization and quantitatively by analysing internal organ masses. Overall, the newly generated phantoms appear very reasonable and representative of the main characteristics of the paediatric population at various ages and for different genders, body sizes and sitting stature ratios. The mass of internal organs increases with height

and body mass. The comparison of organ masses of the heart, kidney, liver, lung and spleen with published autopsy and ICRP reference data for children demonstrated that they follow the same trend when correlated with age. The constructed hybrid computational phantom library opens up the prospect of comprehensive radiation dosimetry calculations and risk assessment for the paediatric population of different age groups and diverse anthropometric parameters.

Keywords: computational phantoms, anthropomorphic, surface representation, paediatric population, library

S Supplementary material for this article is available online

(Some figures may appear in colour only in the online journal)

1. Introduction

The past two decades have witnessed an expansion of various imaging modalities and their application in personalized or precision medicine for evaluating the therapeutic effect of treatment and staging and diagnosing disease (Denecke and Spreckelsen 2013). As a consequence, the exposure to ionizing radiation from medical procedures increased by a factor of seven compared to the early 80's according to the National Council on Radiation Protection and Measurements (NCRP) and the effective dose due to medical radiation exposure per individual has increased from 0.53 to 3.0 mSv (Schauer and Linton 2009). The growing usage of computed tomography (CT) and nuclear medicine procedures is considered to play a pivotal role and stands as the dominant contributor to global radiological warning. The contribution of these two imaging modalities accounts for 36% of the total radiation exposure and 75% of the medical radiation exposure (Schauer 2011). The risk of radiation-induced stochastic and deterministic effects associated with medical radiation procedures and the communication of risks to patients has been a matter of concern in clinical practice, especially for the paediatric population (Hendee and O'Connor 2012, Thornton *et al* 2015). At the same absolute level of absorbed dose, children may experience greater stochastic effects from ionizing radiation than adults (Robbins 2008) and since they have developing organs and longer post-irradiation lifespan, they also suffer greater cancer risk from exposure to ionizing radiation compared to adults (Steinert *et al* 2003). Statistical and computational techniques, such as Monte Carlo-based radiation transport simulation, represent useful tools for providing an accurate assessment of the absorbed dose in the human body since they can account for all aspects of particle interactions within 3D heterogeneous media, simulate a variety of different medical procedures and provide detailed information about energy deposited at the organ/tissue level (Zaidi 1999, Sarrut *et al* 2014). Monte Carlo calculations usually incorporate detailed geometries in the form of computational phantoms to simulate radiation transport and determine the energy pattern of radiation interactions. The reliability and confidence in Monte Carlo simulations is closely related to the degree of realism adopted for computational models, which reflects the physical characteristics (such as elemental composition and mass density, etc) and anatomical features (such as shape, density, volume and position of organs and tissues) of the human body. Depending on the geometric features used to define the anatomical model for radiation transport calculations, computational models can be divided into three types (Zaidi and Xu 2007): (i) stylized models which employ simple equation-based mathematical functions, (ii) voxel-based models which use matrices obtained from segmented cryosection or structural

medical (CT or MR) images, (iii) hybrid equation-voxel based models which combine the two aforementioned modelling approaches, and (iv) anatomical textbook-based, which apply 3 D modelling techniques to data taken from anatomical atlases and textbooks. To represent the human body of different habitus, few computational phantom libraries have been reported. One of the first libraries of human 3D models was developed by Ben Azouz *et al* (2006) consisting of_ENREF_11 constructed surface models with only contours based on anthropometric data from the CAESAR survey (Robinette *et al* 1999). Johnson *et al* (2009) developed a library of phantoms consisting of 15 different paediatric female phantoms and 25 different adult male phantoms by combining the paediatric female phantom and adult male phantom of the University of Florida (Lee *et al* 2009) with published statistical data (standing height, sitting height and body mass, etc) of the US National Health and Nutrition Examination Surveys (NHANES) survey (McDowell *et al* 2008). Na *et al* (2010) developed 5th, 50th and 95th mass and height percentile adult phantoms of both genders based on the Rensselaer Polytechnic Institute (RPI) adult female (RPI-AF) and adult male (RPI-AM) models and the US NHANES survey data, and investigated their dosimetric characteristics for external photon exposure. Stabin *et al* developed a set of reference adult and paediatric phantoms (Stabin *et al* 2012) as well as a series of 10th, 25th, 50th, 75th and 90th height percentile phantoms (Marine *et al* 2010) and obese phantoms (Clark *et al* 2010) to study the effect of stature and mass on specific absorbed fractions (SAFs). Using body parameters representative of people with different size and reported mass-height function from autopsy data, Cassola *et al* (2011) developed 18 anthropometric standing adult Caucasian phantoms with 10th, 50th and 90th mass and height percentiles based on the third edition of standing Female Adult meSH (FASH3) and Male Adult meSH (MASH3) phantoms (Cassola *et al* 2009), and calculated organ equivalent dose and photon SAFs from external and internal exposure, respectively. The Virtual Population (ViP) phantom library, developed at the IT'IS Foundation, represents a library of boundary representation anatomical models created by segmenting more than 300 tissues and organs in whole body magnetic resonance images (MRI) of volunteers, ranging from newborn, paediatric, adult to elderly subjects and including an obese male and a pregnant woman (Gosselin *et al* 2014). To increase the population and application coverage, i.e. to create phantoms with different body mass index (BMI) or postures, several methods were developed and have been integrated in the simulation platform Sim4Life (Cherubini *et al* 2009, Neufeld *et al* 2011). The ViP computational phantoms are frequently used for research and safety evaluations in non-ionizing applications, in particular for mobile phone, MRI and implant safety. Following a different approach, Segars *et al* (2013) constructed a database of Non-Uniform Rational B-Spline (NURBS)-based phantoms consisting of 42 paediatric models and 58 adult models covering a wide distribution of ages, mass and BMI ranges of the population. Unlike the previously mentioned approaches, these models were derived from data of two initial adult models, using non-linear image registration techniques to deform the torso region to approximate image data from patients. While this strategy does not parametrize the population according to BMI, height or standing height and sitting height/stature ratio (SSR), it allows the generation of a large set of different models with torso features and inter-subject variability. A drawback of the approach used to generate the models is that while it generates paediatric models using paediatric image data, it does so by morphing segmented adult models (Segars *et al* 2013). Both Segars' and Stabin's phantom libraries were used for imaging physics research and radiation dosimetry studies (Bond *et al* 2012, Stabin *et al* 2012). Monte Carlo simulations coupled with realistic phantom libraries can provide organ and tissue absorbed dose estimations for a range of masses and habitus of subjects. Interpolating the estimated dose for the actual anthropometric parameters of a subject between the closest data points of the grid, enables accurate assessment of subject-specific organ dose, effective dose and associated cancer risks.

Table 1. Targeted anthropometric parameters for the construction of the hybrid paediatric phantom library. The mass is provided in kg, length is given in cm.

Anthropometric parameters		Percentiles				
		10	25	50	75	90
Newborn-female	Mass	2.7	3.1	3.4	3.7	4.0
	Length	46.3	47.7	49.3	51.0	52.7
Newborn-male	Mass	2.8	3.2	3.5	3.9	4.2
	Length	46.6	48.2	50.0	51.8	53.4
1 year-female	Mass	8.8	9.9	10.9	11.9	13
	Length	70.6	72.4	74.4	76.4	78.1
1 year-male	Mass	9.2	10.5	11.5	12.6	13.8
	Length	72.5	74.2	76.1	78.2	80.1
2 years-female	Mass	10.7	12.1	13.1	14.4	16.1
	Height	84	87.2	90.2	93.2	95.6
	SSR	53.5	54.7	55.9	57.2	58.4
2 years-male	Mass	12	12.8	13.9	15.1	16.4
	Height	86.9	89.2	91.9	94.5	96.8
	SSR	54.4	55.6	56.9	58.3	59.6
5 years-female	Mass	15.9	17.6	19.6	22.1	25.5
	Height	105.2	107.4	111.7	116.6	119.6
	SSR	51.1	52.5	53.6	54.7	55.8
5 years-male	Mass	17.4	18.9	21	23.5	26.9
	Height	107	111.4	114.6	117.9	120.8
	SSR	51.4	52.4	53.5	54.6	55.7
10 years-female	Mass	29.1	32.5	40.5	49	58.5
	Height	135	138.6	143.7	148.7	152.8
	SSR	50	50.9	51.9	52.9	53.9
10 years-male	Mass	28.4	31.7	37.3	45.1	56.8
	Height	133	136.8	141.5	147	151.3
	SSR	49.3	50.2	51.2	52.2	53.1
15 years-female	Mass	46.5	50.7	57.6	67.6	81
	Height	154.3	158.4	162	165.8	170.1
	SSR	50	50.8	51.8	52.8	53.7
15 years-male	Mass	52.4	58.2	66.3	76.9	89.9
	Height	163.5	169.2	174.8	178	182
	SSR	49.3	50.2	51.1	52.2	53.1

In this work, a methodology and a computer code were developed to use hybrid and voxel-based phantoms to construct a broad library of paediatric phantoms covering statistical distributions of body morphometry of the paediatric population. The 10th, 25th, 50th, 75th and 90th percentiles of body anthropometric parameters, including body mass, length, standing height and SSR were used to remodel the reference phantoms based on an existing set of IT'IS paediatric phantoms (Gosselin *et al* 2014). A total of 1100 anthropometric computational phantoms were produced for a newborn (25 phantoms for each gender) as well as 1 year (25 phantoms for each gender), 2 years (125 phantoms for each gender), 5 years (125 phantoms for each gender), 10 years (125 phantoms for each gender) and 15 years-old (125 phantoms for each gender) female and male children, respectively.

Table 2. The ICRP reference phantoms are constructed from a set of phantoms from the Virtual Population. The model used for each reference phantom is shown.

Reference phantom	IT'IS phantom
Newborn-female	Charlie
Newborn-male	Charlie
1 year-female	Nina
1 year-male	Nina
2 years-female	Nina
2 years-male	Nina
5 years-female	Roberta
5 years-male	Roberta
10 years-female	Billie
10 years-male	Billie
15 years-female	Billie
15 years-male	Louis

Table 3. Standing height, body mass, BMI and SSR for the original paediatric IT'IS phantom series.

Anthropometric parameters	Newborn		1 year-old		5 years-old.		10 years-old		15 years-old	
	Female	Male	Female	Male	Female	Male	Female	Male	Female	Male
Standing height	52.8	53.2	78.8	78.8	113.5	113.4	144.3	144.4	168	174.8
Body mass	3.5	3.5	10.0	10.0	19.0	19.0	31.8	31.6	53.2	55.8
BMI	12.5	12.2	16.0	16.1	14.7	14.8	15.3	15.2	18.9	18.3
SSR	—	—	—	—	0.62	0.62	0.51	0.52	0.53	0.52

2. Materials and methods

2.1. Datasets and anthropometric parameters

NHANES conducted in the US by the Centers for Disease Control (CDC) and Prevention's National Center for Health Statistics (NCHS) are the primary source of body measurement and related health and nutrition data for the US population. The 2003–2006 datasets of anthropometric reference data for children and adults were released in 2008 and are available on the CDC web site[7] (McDowell *et al* 2008). The current paper is based on the body measurement examinations of 19 593 persons from these datasets and provides the 10th, 25th, 50th, 75th and 90th percentiles of the mass and standing height data corresponding to children of 2, 5, 10, and 15 years, respectively, and the mass and recumbent length data corresponding to a newborn and 1 year-old child. The SSR values used in this work for the paediatric population older than 1 year were retrieved from the NHANES III survey (1988–1994) examination data (Frisancho 2008).

A number of anthropometric parameters can be used for the generation of the phantom libraries, including standing height, sitting height, body mass, body mass index (BMI), SSR, waist, arm/thigh circumference, arm length and skinfold, etc. The body height, weight and BMI were reported to have statistical correlations with some organs in autopsy-based anthropometric studies (de la Grandmaison *et al* 2001a, Sheikhazadi *et al* 2010, Molina and DiMaio

[7] www.cdc.gov

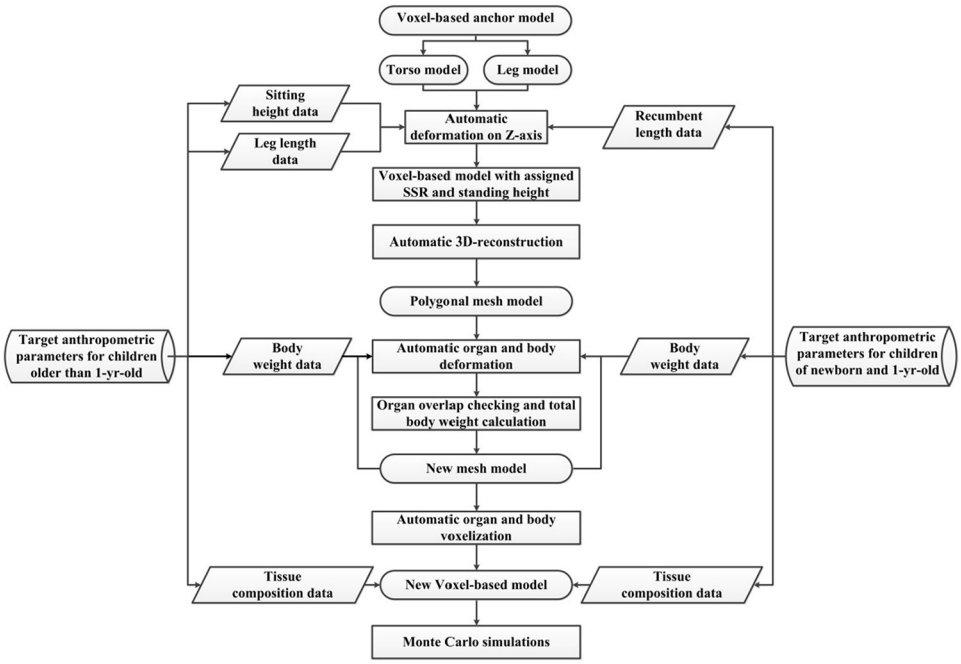

Figure 1. Flowchart of the phantom modelling process adopted for generation of new computational models. The target anthropometric parameters are obtained from the NHANES database, the anchor phantoms are remodelled into a new model with the desired anatomical parameters.

2015). In this work, we selected the body mass, standing height and SSR as general indicators for body morphometry of a subject since these parameters can be easily manipulated within the automatic process and have an important impact on radiation dosimetry calculations.

Total body mass and standing height represent general indicators for the size of a subject and characterize the percentage of body fat. In order to determine target values, a fine grid data is created from body mass and standing height distributions of each paediatric database. With the determined body mass and standing height, the BMI can be calculated as $\mathrm{BMI} = \mathrm{body\ weight} / \mathrm{standing\ height}^2$. The standing height limits the variability in both sitting height and leg length. The sitting height and leg length are calculated as $\mathrm{standing\ height} \times \mathrm{SSR}$ and $\mathrm{standing\ height} \times (1 - \mathrm{SSR})$, respectively. For children younger than 2 years, the NHANES database does not include standing height or SSR data, so the body mass and recumbent length are used to parameterize the newborn and 2 years-old population. The list of target anthropometric parameters for paediatric females and males of each age group are summarized in table 1.

2.2. Anchor phantoms

The IT'IS phantom series (Gosselin *et al* 2014) includes a series of paediatric models from the newborn to a 14 years-old adolescent (Charlie of representing a newborn male model, Nina representing a 3 years-old female model, Roberta representing a 5 years-old female model, Billie representing an 11 years-old female model, and Louis representing a 14 years-old male model). However, the models do not fit the body and organ masses recommended by the International Commission on Radiological Protection (ICRP) for the reference paediatric

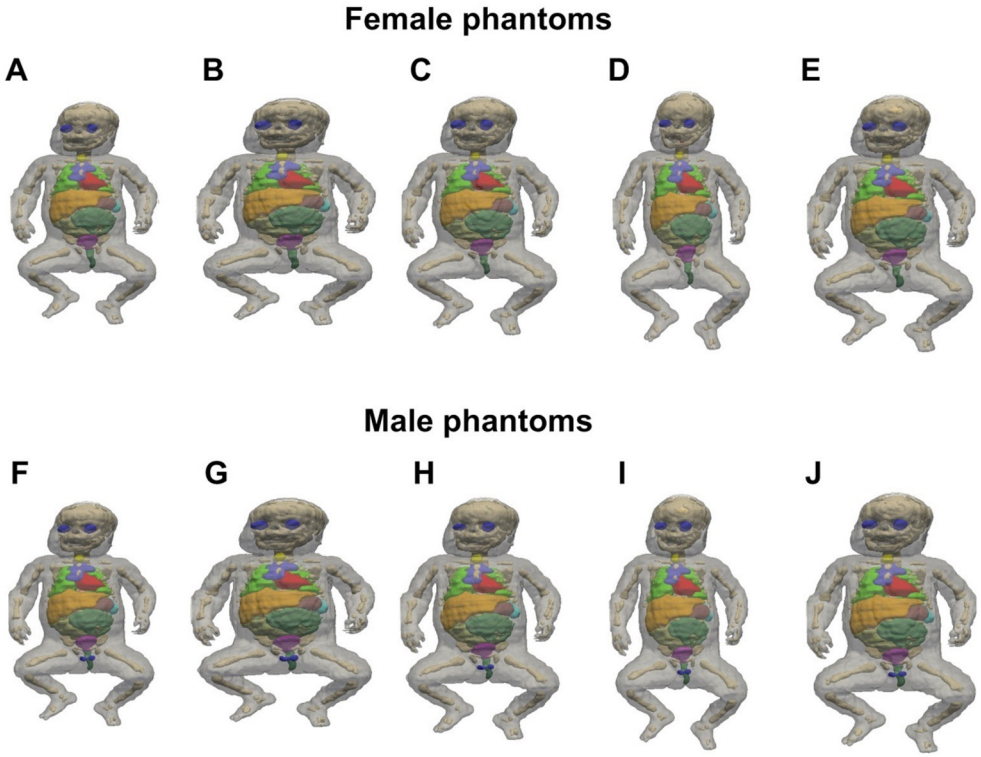

Figure 2. 3D visualization of representative computational phantoms of the newborn: (A) 10th mass, 10th length female (F-newborn-10m-10l); (B) 90th mass, 10th length female (F-newborn-90m-10l); (C) 50th mass, 50th length female (F-newborn-50m-50l); (D) 10th mass, 90th length female (F-newborn-10m-90l); (E) 90th mass, 90th length female (F-newborn-90m-90l); (F) 10th mass, 10th length male (M-newborn-10m-10l); (G) 90th mass, 10th length male (M-newborn-90m-10l); (H) 50th mass, 50th length male (M-newborn-50m-50l); (I) 10th mass, 90th length male (M-newborn-10m-90l); (J) 90th mass, 90th length male (M-newborn-90m-90l). (Red for the heart, light green for the lung, yellow for the liver, dark green for colon, violet for UB.)

population. In this context, we first constructed a series of reference paediatric phantoms based on the IT'IS dataset fitting the ICRP (report 89) reference anatomical data (ICRP 2002). These generated reference phantoms are used as representative anchor phantoms to be modelled to generate models of the newborn, 1-, 5-, 10-, and 15 years-old female and male children, respectively (table 2). The 5 years-old reference phantoms were used as anchor phantoms for 2 years-old population. A united voxel dimension of $2 \times 2 \times 3\,\mathrm{mm}^3$ was set for all anchor models to minimize the differences across different models. The cartilage, cortical bone, and spongiosa at different bone sites were combined. The spongiosa is treated as a mixture of active marrow, inactive marrow, and trabecular bone.

Since the ICRP recommends the same tissue weighting factors for homogeneous organs, such as the left lung and the right lung, we merged them as one identified region for convenient effective dose calculation. The blood vessel in the phantom refers to the blood in the arteries and the veins. The kidney cortex, kidney medulla and kidney pelvis were merged as kidney. A total of 43 organs and tissues are included in the reference phantoms. The original body mass, standing height, BMI and SSR for the newborn, 1-, 5-, 10-, and 15 years-old female and male anchor phantoms are summarized in table 3.

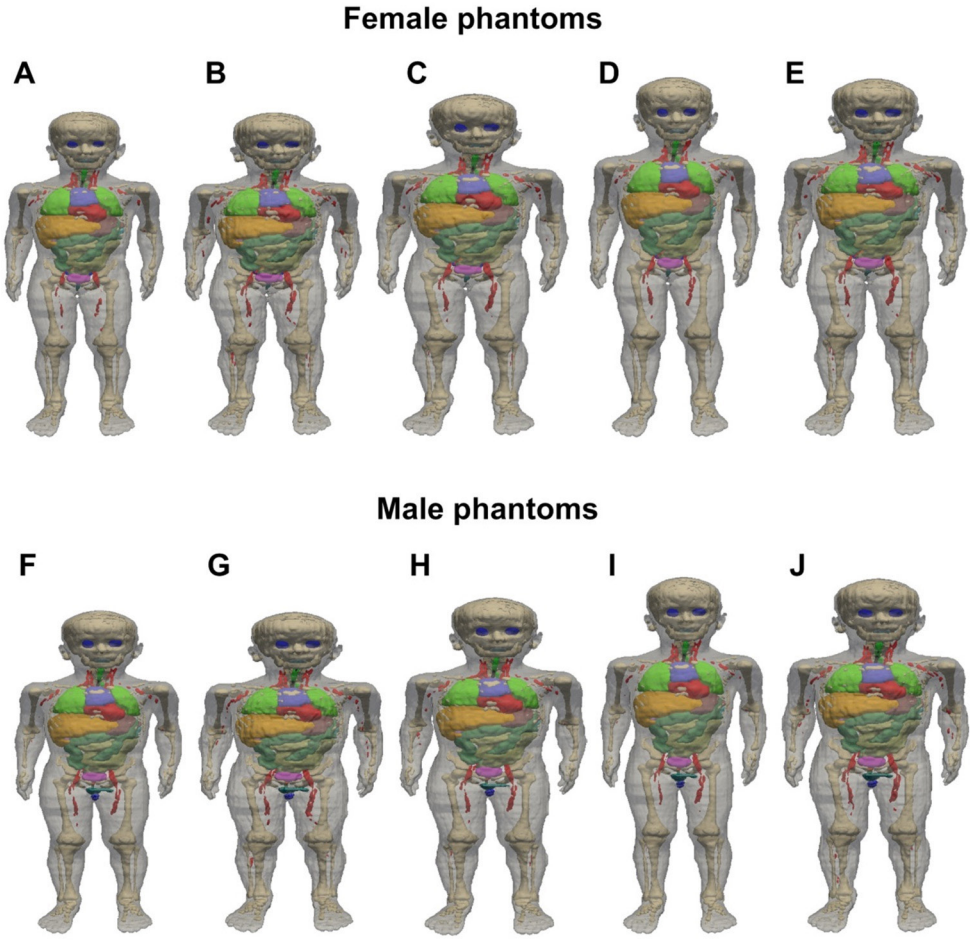

Figure 3. 3D visualization of representative computational phantoms of the 1 year-old: (A) 10th mass, 10th length female (F-01y-10m-10l); (B) 90th mass, 10th length female (F-01y-90m-10l); (C) 50th mass, 50th length female (F-01y-50m-50l); (D) 10th mass, 90th length female (F-01y-10m-90l); (E) 90th mass, 90th length female (F-01y-90m-90l); (F) 10th mass, 10th length male (M-01y-10m-10l); (G) 90th mass, 10th length male (M-01y-90m-10l); (H) 50th mass, 50th length male (M-01y-50m-50l); (I) 10th mass, 90th length male (M-01y-10m-90l); (J) 90th mass, 90th length male (M-01y-90m-90l). (Red for the heart, light green for the lung, yellow for the liver, dark green for colon, violet for UB.)

2.3. Model generation

The schematic flowchart shown in figure 1 illustrates the modelling process. The deformation process used in this work consists of three basic components: (i) the target anthropometric parameters obtained from the NHANES database, (ii) the anchor phantoms with well-defined anatomical structures that match reference data of the paediatric population; and (iii) the software tools that reconstruct polygon mesh models from voxel-based models, modelling the mesh phantom into a new one according to desired anatomical parameters. Thereafter, the generated mesh model is voxelized into a new voxel-based model that can be used as input for Monte Carlo calculations. For children older than 1 year, sitting height and leg

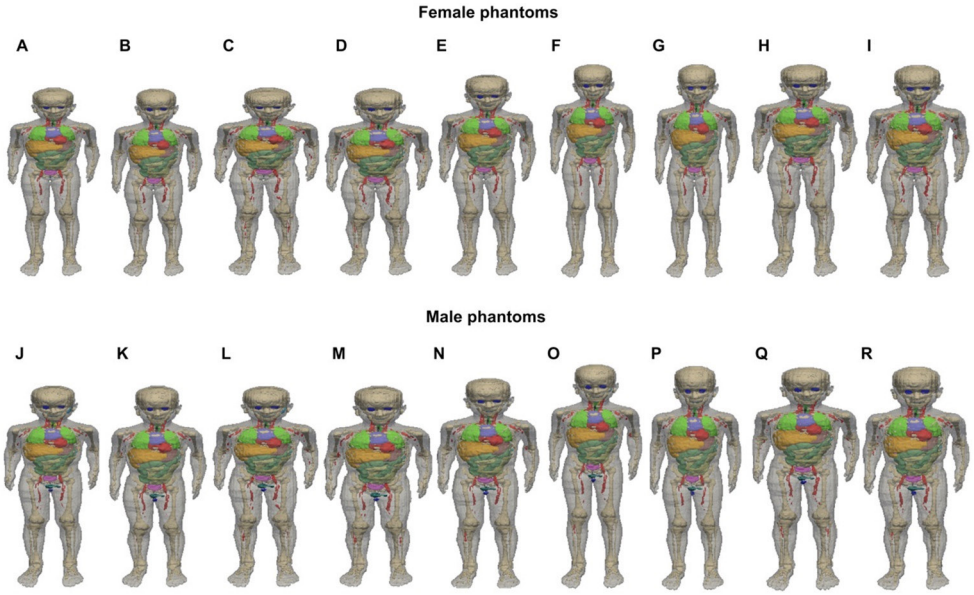

Figure 4. 3D visualization of representative computational phantoms of the 2 years-old: (A) 10th mass, 10th height and 10th SSR female (F-02y-10m-10h-10S); (B) 10th mass, 10th height and 90th SSR female (F-02y-10m-10h-90S); (C) 90th mass, 10th height and 10th SSR female (F-02y-90m-10h-10S); (D) 90th mass, 10th height and 90th SSR female (F-02y-90m-10h-90S); (E) 50th mass, 50th height and 50th SSR female (F-02y-50m-50h-50S); (F) 10th mass, 90th height and 10th SSR female (F-02y-10m-90h-10S); (G) 10th mass, 90th height and 90th SSR female (F-02y-10m-90h-90S); (H) 90th mass, 90th height and 10th SSR female (F-02y-90m-90h-10S); (I) 90th mass, 90th height and 90th SSR female (F-02y-90m-90h-90S); (J) 10th mass, 10th height and 10th SSR male (M-02y-10m-10h-10S); (K) 10th mass, 10th height and 90th SSR male (M-02y-10m-10h-90S); (L) 90th mass, 10th height and 10th SSR male (M-02y-90m-10h-10S); (M) 90th mass, 10th height and 90th SSR male (M-02y-90m-10h-90S); (N) 50th mass, 50th height and 50th SSR male (M-02y-50m-50h-50S); (O) 10th mass, 90th height and 10th SSR male (M-02y-10m-90h-10S); (P) 10th mass, 90th height and 90th SSR male (M-02y-10m-90h-90S); (Q) 90th mass, 90th height and 10th SSR male (M-02y-90m-90h-10S); (R) 90th mass, 90th height and 90th SSR male (M-02y-90m-90h-90S). (Red for the heart, light green for the lung, yellow for the liver, dark green for colon, violet for UB.)

length values were determined from targeted mass, standing height and SSR. The voxel-based anchor phantom is divided into torso and leg parts. The targeted sitting height and leg length are matched by uniformly scaling the torso (including the head, arms, regional skeleton and organs) and the leg (including all regional skeleton and tissues) using an in-house developed C++ code. With sitting height and leg length being adjusted to achieve the target values, the new torso and leg models are merged into a new voxel model with the desired SSR and standing height, which is then automatically reconstructed into a polygon mesh model using an in-house code based on the visualization toolkit (VTK). The next step in phantom modification is to match the targeted total body mass. For the 10th, 25th, 50th, 75th and 90th weight percentile phantoms, the desired mass is achieved by scaling the mesh model in two dimensions. This process involves iterating between the evaluation of total body mass and adjustment of the scaling factors for internal organs and body contour. The gaps between organs generated during the scaling process were filled with adipose tissue and the overlaps occuring between organs assigned to the organ having the smaller volume. The

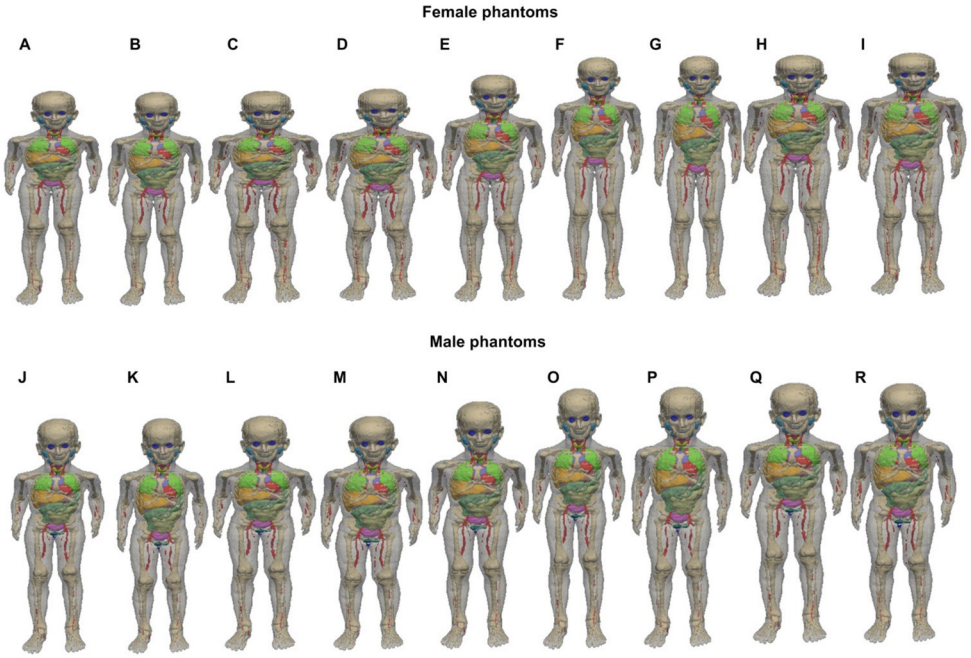

Figure 5. 3D visualization of representative computational phantoms of the 5 years-old: (A) 10th mass, 10th height and 10th SSR female (F-05y-10m-10h-10S); (B) 10th mass, 10th height and 90th SSR female (F-05y-10m-10h-90S); (C) 90th mass, 10th height and 10th SSR female (F-05y-90m-10h-10S); (D) 90th mass, 10th height and 90th SSR female (F-05y-90m-10h-90S); (E) 50th mass, 50th height and 50th SSR female (F-05y-50m-50h-50S); (F) 10th mass, 90th height and 10th SSR female (F-05y-10m-90h-10S); (G) 10th mass, 90th height and 90th SSR female (F-05y-10m-90h-90S); (H) 90th mass, 90th height and 10th SSR female (F-05y-90m-90h-10S); (I) 90th mass, 90th height and 90th SSR female (F-05y-90m-90h-90S); (J) 10th mass, 10th height and 10th SSR male (M-05y-10m-10h-10S); (K) 10th mass, 10th height and 90th SSR male (M-05y-10m-10h-90S); (L) 90th mass, 10th height and 10th SSR male (M-05y-90m-10h-10S); (M) 90th mass, 10th height and 90th SSR male (M-05y-90m-10h-90S); (N) 50th mass, 50th height and 50th SSR male (M-05y-50m-50h-50S); (O) 10th mass, 90th height and 10th SSR male (M-05y-10m-90h-10S); (P) 10th mass, 90th height and 90th SSR male (M-05y-10m-90h-90S); (Q) 90th mass, 90th height and 10th SSR male (M-05y-90m-90h-10S); (R) 90th mass, 90th height and 90th SSR male (M-05y-90m-90h-90S). (Red for the heart, light green for the lung, yellow for the liver, dark green for colon, violet for UB.)

organ mass is calculated as the product of the organ volume and corresponding organ density of the paediatric population at various ages (ICRP 2002). The total body mass is determined as the sum of masses of all identified organs and residual tissue. The final step for computational phantom development is to re-voxelize the generated new mesh model into voxel model using an in-house developed C++ code. The entire phantom deformation process is completed automatically according to the targeted anthropometric parameters and given anchor phantoms. The generated phantoms were evaluated qualitatively using 3D visualization and quantitatively by analysing internal organ masses.

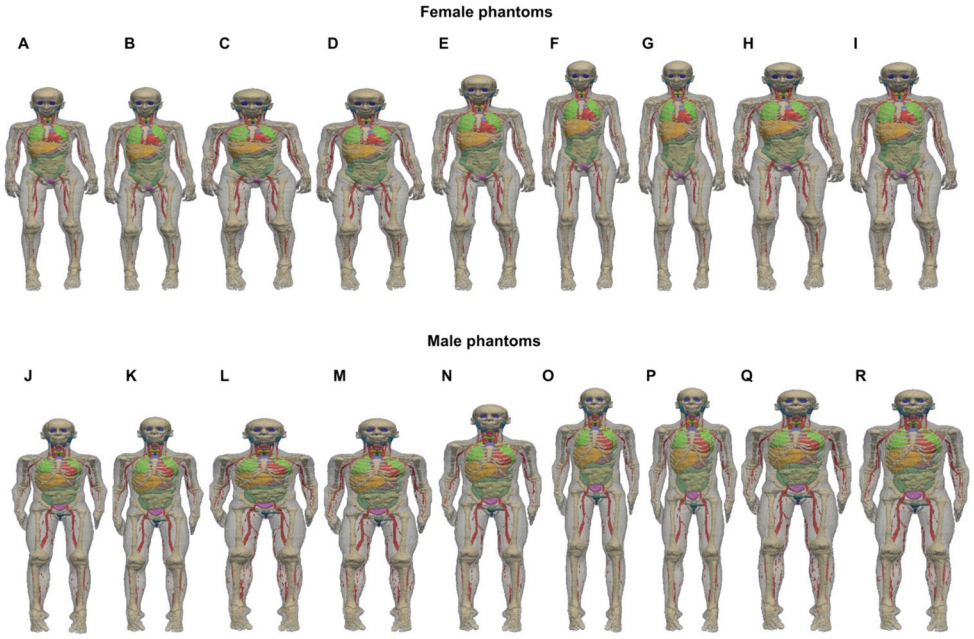

Figure 6. 3D visualization of representative computational phantoms of the 10 years-old: (A) 10th mass, 10th height and 10th SSR female (F-10y-10m-10h-10S); (B) 10th mass, 10th height and 90th SSR female (F-10y-10m-10h-90S); (C) 90th mass, 10th height and 10th SSR female (F-10y-90m-10h-10S); (D) 90th mass, 10th height and 90th SSR female (F-10y-90m-10h-90S); (E) 50th mass, 50th height and 50th SSR female (F-10y-50m-50h-50S); (F) 10th mass, 90th height and 10th SSR female (F-10y-10m-90h-10S); (G) 10th mass, 90th height and 90th SSR female (F-10y-10m-90h-90S); (H) 90th mass, 90th height and 10th SSR female (F-10y-90m-90h-10S); (I) 90th mass, 90th height and 90th SSR female (F-10y-90m-90h-90S); (J) 10th mass, 10th height and 10th SSR male (M-10y-10m-10h-10S); (K) 10th mass, 10th height and 90th SSR male (M-10y-10m-10h-90S); (L) 90th mass, 10th height and 10th SSR male (M-10y-90m-10h-10S); (M) 90th mass, 10th height and 90th SSR male (M-10y-90m-10h-90S); (N) 50th mass, 50th height and 50th SSR male (M-10y-50m-50h-50S); (O) 10th mass, 90th height and 10th SSR male (M-10y-10m-90h-10S); (P) 10th mass, 90th height and 90th SSR male (M-10y-10m-90h-90S); (Q) 90th mass, 90th height and 10th SSR male (M-10y-90m-90h-10S); (R) 90th mass, 90th height and 90th SSR male (M-10y-90m-90h-90S). (Red for the heart, light green for the lung, yellow for the liver, dark green for colon, violet for UB.)

3. Results

Representative images of the constructed paediatric phantoms of different anthropometric parameters are shown in figures 2–7, where the skin, muscle and adipose tissue are set to transparent for better visualization of the internal organs. Figures 2 and 3 show both female and male models with 10th and 90th mass, 10th and 90th body length, as well as models with 50th mass and 50th body length for the newborn and 1 year-old child, respectively. The naming of the constructed phantoms of the newborn and 1 year-old child follows the moniker where the anchor phantom of the corresponding age group is successively subscripted by the gender, weight percentile and recumbent length percentile. Figures 4–7 illustrate both female and male models with 10th and 90th mass, 10th and 90th standing height, 10th and 90th SSR, as well as models with 50th mass, 50th standing height, 50th SSR for the 2 years-old, 5

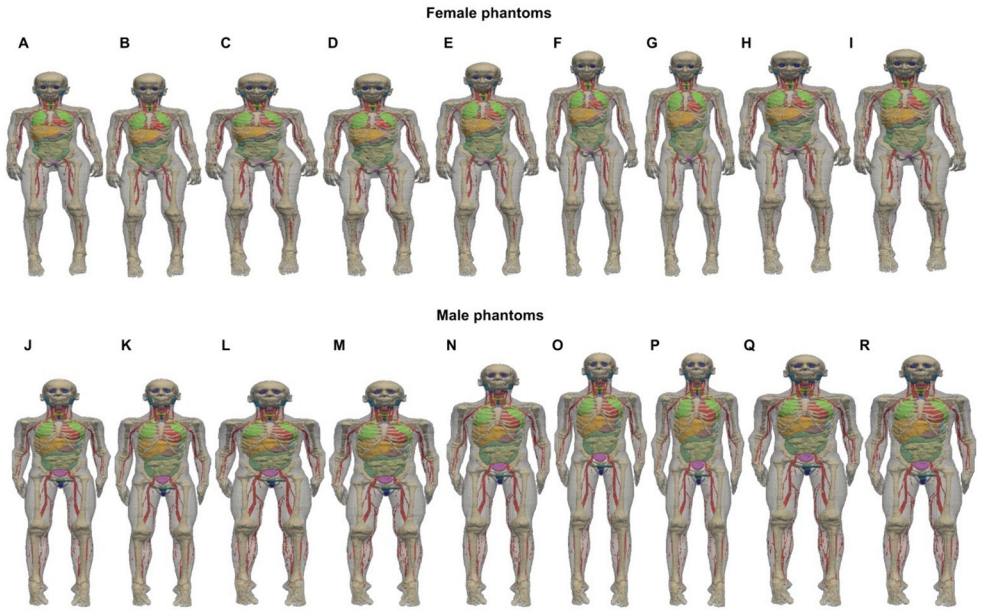

Figure 7. 3D visualization of representative computational phantoms of the 15 years-old: (A) 10th mass, 10th height and 10th SSR female (F-15y-10m-10h-10S); (B) 10th mass, 10th height and 90th SSR female (F-15y-10m-10h-90S); (C) 90th mass, 10th height and 10th SSR female (F-15y-90m-10h-10S); (D) 90th mass, 10th height and 90th SSR female (F-15y-90m-10h-90S); (E) 50th mass, 50th height and 50th SSR female (F-15y-50m-50h-50S); (F) 10th mass, 90th height and 10th SSR female (F-15y-10m-90h-10S); (G) 10th mass, 90th height and 90th SSR female (F-15y-10m-90h-90S); (H) 90th mass, 90th height and 10th SSR female (F-15y-90m-90h-10S); (I) 90th mass, 90th height and 90th SSR female (F-15y-90m-90h-90S); (J) 10th mass, 10th height and 10th SSR male (M-15y-10m-10h-10S); (K) 10th mass, 10th height and 90th SSR male (M-15y-10m-10h-90S); (L) 90th mass, 10th height and 10th SSR male (M-15y-90m-10h-10S); (M) 90th mass, 10th height and 90th SSR male (M-15y-90m-10h-90S); (N) 50th mass, 50th height and 50th SSR male (M-15y-50m-50h-50S); (O) 10th mass, 90th height and 10th SSR male (M-15y-10m-90h-10S); (P) 10th mass, 90th height and 90th SSR male (M-15y-10m-90h-90S); (Q) 90th mass, 90th height and 10th SSR male (M-15y-90m-90h-10S); (R) 90th mass, 90th height and 90th SSR male (M-15y-90m-90h-90S). (Red for the heart, light green for the lung, yellow for the liver, dark green for colon, violet for UB.)

years-old, 10 years-old and 15 years-old paediatric models, respectively. The naming of the developed phantoms of the 2, 5, 10, and 15 years-old children follows the moniker whereby the anchor phantom of corresponding age group is successively subscripted by the gender, weight percentile, standing height percentile and SSR percentile. The organ mass of 1100 remodelled computational phantoms was calculated (see supplemental material) (stacks.iop.org/PMB/62/3263/mmedia).

Table 4 shows the Pearson correlation coefficients of the relationship between age and body habitus (mass and length for the newborn and 1 year-old child and mass, height, BMI and SSR for children older than 1 year) and mass of representative organs of the constructed paediatric phantoms. The Pearson correlation coefficient ρ is calculated as: $\rho_{(a,b)} = \mathrm{cov}_{(a,b)}/(\sigma_a \times \sigma_b)$, where *cov* is the covariance of two investigated variables and σ is the standard deviation. Overall, the organ mass increases with body mass, recumbent length, body height and BMI and decreases with SSR, except for the adrenals. Consistent with observations made in

Table 4. Pearson correlation coefficients of the relationship between body habitus (mass, height, BMI, SSR and Sitting Height) and mass of representative organs of the constructed paediatric phantoms (SI: small intestine; UB: urinary bladder; GB: gall bladder).

	Newborn and 1 year-old children			Children older than 1 year-old				
Organs	Age	Height	Length	Age	Height	Mass	BMI	SSR
Adipose tissue	0.87	0.83	0.90	0.90	0.86	0.98	0.78	−0.58
Adrenal	−0.75	−0.76	−0.60	0.75	0.74	0.93	0.84	−0.41
Brain	0.95	0.94	0.99	0.34	0.34	0.57	0.78	−0.37
Colon	0.89	0.87	0.96	0.89	0.88	0.98	0.79	−0.60
GB	0.87	0.87	0.95	0.86	0.87	0.97	0.75	−0.55
Heart	0.94	0.92	0.99	0.88	0.87	0.99	0.80	−0.55
Kidney	0.95	0.93	1.00	0.84	0.83	0.97	0.82	−0.52
Esophagus	0.93	0.91	0.98	0.91	0.89	1.00	0.78	−0.58
Liver	0.95	0.92	0.99	0.88	0.86	0.99	0.81	−0.54
Lung	0.93	0.91	0.99	0.89	0.89	0.99	0.77	−0.56
Pancreas	0.96	0.94	1.00	0.90	0.88	0.99	0.78	−0.55
Salivary glands	0.57	0.60	0.62	0.87	0.85	0.94	0.77	−0.62
SI	0.95	0.93	1.00	0.89	0.89	0.97	0.78	−0.60
Spinal cord	0.55	0.50	0.54	0.78	0.75	0.90	0.76	−0.51
Spleen	0.94	0.92	0.99	0.89	0.88	0.99	0.79	−0.55
Stomach	0.70	0.67	0.83	0.89	0.89	0.98	0.78	−0.61
Thymus	0.94	0.92	0.99	0.07	0.10	0.36	0.63	0.05
Thyroid	0.18	0.23	0.26	0.92	0.89	0.98	0.77	−0.65
UB	0.91	0.89	0.97	0.86	0.85	0.97	0.80	−0.54
Blood vessel	0.87	0.87	0.91	0.91	0.90	0.99	0.74	−0.60
Muscle	0.93	0.92	0.97	0.90	0.89	0.99	0.76	−0.60
Cortical bone	0.91	0.88	0.95	0.91	0.88	0.99	0.77	−0.59
Spongiosa	0.94	0.94	0.98	0.92	0.90	1.00	0.77	−0.61
Cartilage	0.90	0.90	0.93	0.92	0.90	0.99	0.76	−0.61
Breast	0.36	0.30	0.33	0.51	0.44	0.49	0.43	−0.27
Bronchi	0.78	0.79	0.83	0.88	0.86	0.94	0.74	−0.54
Eye balls	0.04	0.01	0.09	0.39	0.41	0.48	0.51	−0.47
Larynx	0.95	0.92	0.96	0.85	0.84	0.96	0.78	−0.60
Mucosa	0.89	0.87	0.92	0.79	0.77	0.88	0.74	−0.63
Tongue	0.94	0.91	0.96	0.91	0.87	0.99	0.80	−0.62
Trachea	0.94	0.93	0.96	0.87	0.87	0.98	0.77	−0.56
Skin	0.92	0.89	0.97	0.88	0.84	0.97	0.74	−0.55

published autopsy studies of Caucasoid adults (de la Grandmaison *et al* 2001b), organ masses show better statistical correlations with the body mass and height than the BMI and SSR for children older than 1 year. For the newborn and 1 year-old child, the adrenal mass decreases with age, body mass and length. This is due to the renal growth and involution of the foetal cortex in the first year after birth and the adrenal mass begins to increase, gradually regaining

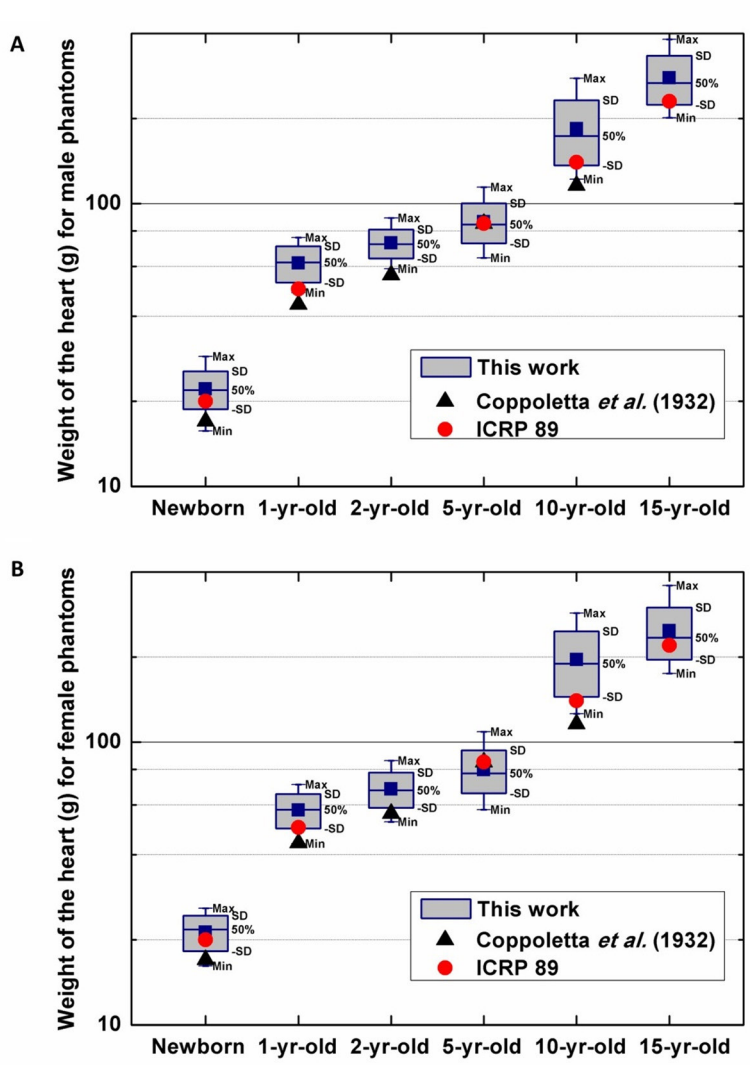

Figure 8. Comparison between heart mass of the constructed male (A) and female (B) paediatric phantoms in this work and reference data of the ICRP 89 (ICRP 2002), and autopsy data of Coppoletta and Wolbach (1933). The squares represent the mean values whereas the 50% horizontal line represents the median values.

its natal mass around puberty after 2 years-old. Figures 8–12 show the maximum, minimum, mean (squares), and median (50% horizontal line) values as well as standard deviations of the estimated organ masses of the heart, kidney, liver, lung and spleen, respectively. The masses of the selected organs increase with increasing age of the children.

4. Discussion

The realistic hybrid computational female and male phantoms developed in this work represent a comprehensive anthropometric paediatric phantom library. The phantoms are very reasonable and realistic as revealed by visual inspection: (i) the heart is located at the

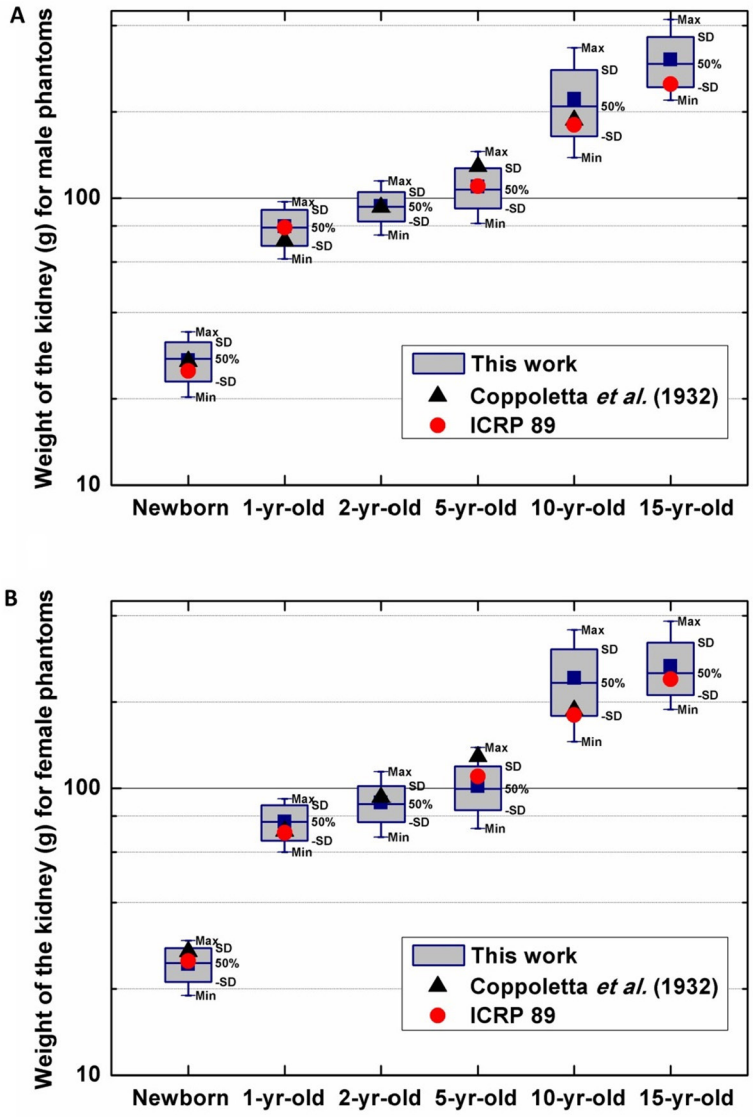

Figure 9. Comparison between kidney mass of the constructed male (A) and female (B) paediatric phantoms in this work and reference data of the ICRP 89 (ICRP 2002), and autopsy data of Coppoletta and Wolbach (1933). The squares represent the mean values whereas the 50% horizontal line represents the median values.

approximate level of the fifth or six rib with about two thirds of the volume in the left of the body midline; (ii) the lung occupy most of the thoracic cavity; (iii) the lateral margin of the liver reaches the mammillary line on the left side; (iv) the arm length extends to the mid-thigh; and (v) the head-body size ratio decreases from 1:4 in the newborn to 1:7 in the 15 years-old adolescent, which reflects the status of the human body undergoing regular allometric growth. However, the combination of some extreme (and partly conflicting) percentiles also results in unrealistic features (unusual head-body ratio) in some phantoms (figure 3(G)). This phantom can be used as extreme case representative of a

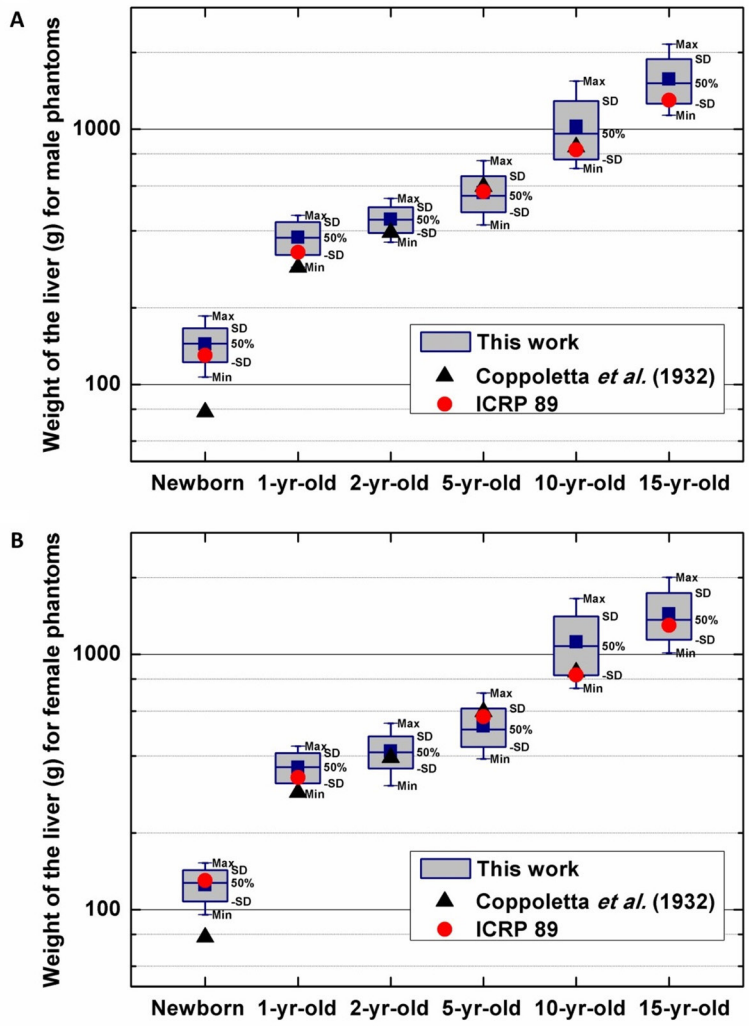

Figure 10. Comparison between liver mass of the constructed male (A) and female (B) paediatric phantoms in this work and reference data of the ICRP 89 (ICRP 2002), and autopsy data of Coppoletta and Wolbach (1933). The squares represent the mean values whereas the 50% horizontal line represents the median values.

limited population for simulation studies of radiographic examinations of the head and neck region.

To evaluate the accuracy of the scaled organ masses, comparisons between organ masses in this work, the reference data of the ICRP 89 (ICRP, 2002) and the autopsy data of Coppoletta and Wolbach (1933) for the paediatric population at various age groups were performed (figures 8–12). In the autopsy study, the masses of vital organs of 1198 autopsies aging from birth to 12 years-old were measured for the paediatric population of the US in the early 1920s. The ICRP 89 reference values were estimated based on the anatomy data of the paediatric population in western Europeans and north Americans obtained from 1970s to 1990s. For the heart, kidney, liver, lung and spleen of female models, the mean organ masses of phantoms in the our newly generated library are about 7–27% and

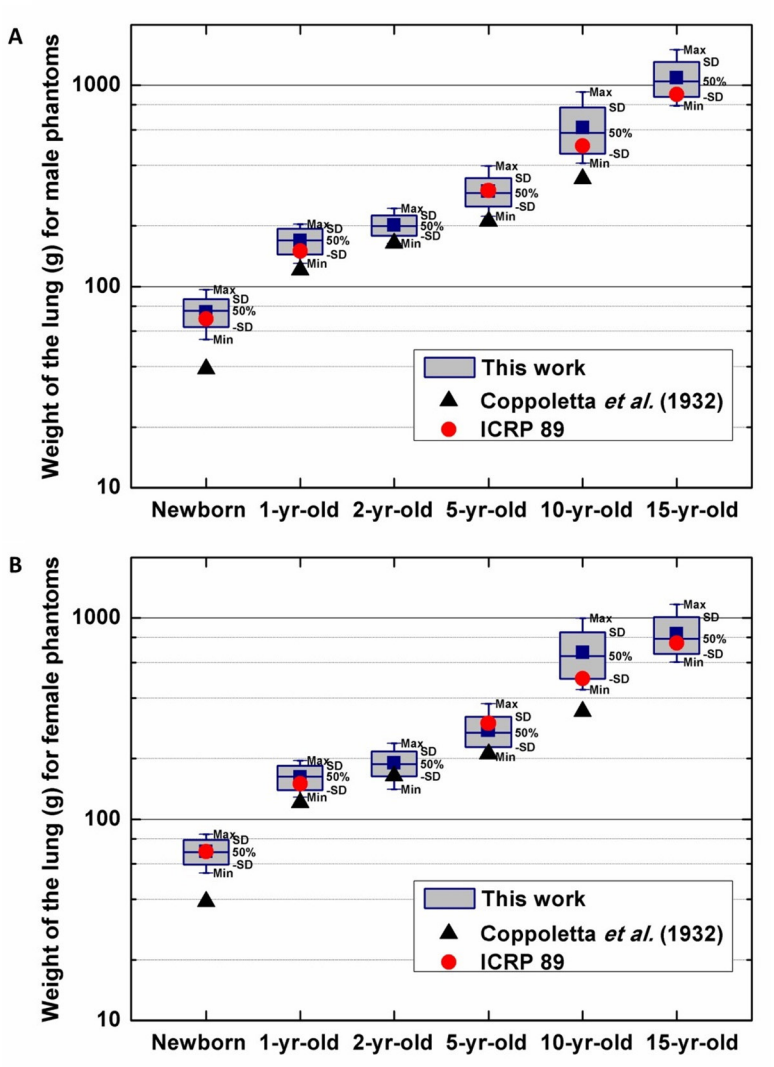

Figure 11. Comparison between lung mass of the constructed male (A) and female (B) paediatric phantoms in this work and reference data of the ICRP 89 (ICRP 2002), and autopsy data of Coppoletta and Wolbach (1933) The squares represent the mean values whereas the 50% horizontal line represents the median values.

4–15% higher than the corresponding values of the autopsy data and ICRP reference data, respectively. For male models of the generated library, the mean organ masses are about 10–30% and 4–14% higher than the corresponding values of the autopsy data and ICRP reference data, respectively. The relatively low organ masses observed in the autopsy study performed in the 1920s is because in the 20th century, the average mass and height of the population in developed countries increased progressively (Caballero 2007). The slightly higher mean organ mass in the remodelled phantoms presented here can be attributed to the higher average body mass and BMI of the NHANES database for the paediatric population at various ages compared to the ICRP reference children data. The higher mean organ mass

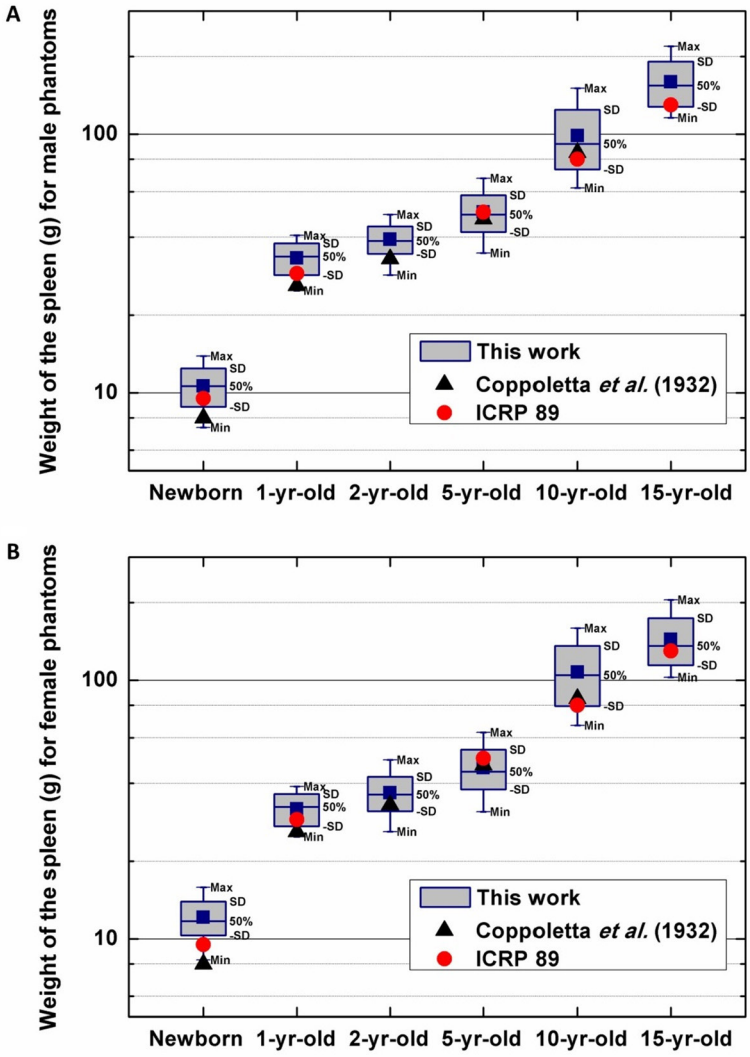

Figure 12. Comparison between spleen mass of the constructed male (A) and female (B) paediatric phantoms in this work and reference data of the ICRP 89 (ICRP 2002), and autopsy data of Coppoletta and Wolbach (1933). The squares represent the mean values whereas the 50% horizontal line represents the median values.

may result in smaller mean self-absorbed organ dose for internal dosimetry and affect the calculated effective dose.

The model generation approach employed in this work provided a fast and easy-to-use modelling method for constructing computational models fitting target anthropometric parameters for radiation dosimetry calculations. However, the original segmentation of IT'IS models was performed with 0.5 mm voxel resolution and as such, the down-scaled voxel size of the original models may cause relevant features loss. The voxel size ($2 \times 2 \times 3\,mm^3$) adopted for the construction of the generated phantoms might introduce small uncertainties ($<1\%$) in Monte Carlo simulations-based internal dosimetry calculations of small organs, such as the thyroid. The linear scaling procedure used during

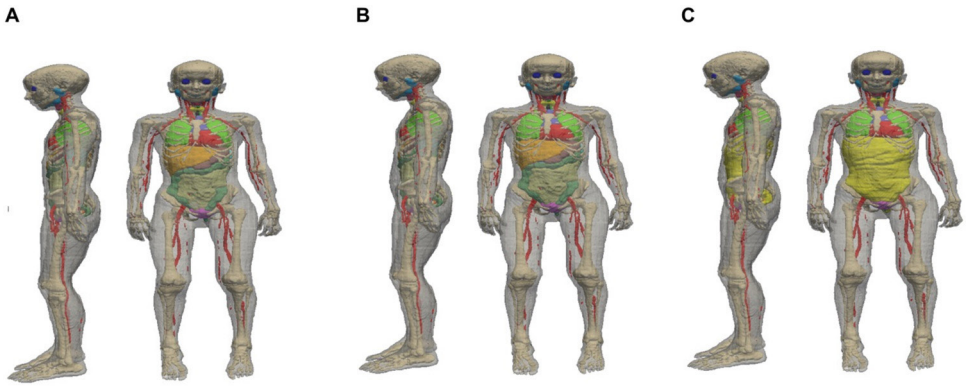

Figure 13. Illustration of (A) the 10 years-old female phantom with 50th mass, 50th height and 50th SSR; (B) 10 years-old obese female phantom and (C) 10 years-old obese female phantom with non-transparent visceral fat (in yellow).

phantoms construction assumes the independence between selected body morphometries. An identical scaling factor is set for longitudinal and transversal axes. The body mass increase of different phantoms is mostly contributed by the increased mass of internal organs and subcutaneous fat. However, these assumptions do not consider the distribution of visceral fat in the abdomen for model construction. In this condition, we developed a module enabling to add the visceral fat in the computational models in the phantom modelling tool (figure 13). Using the developed visceral fat software module, users of the phantom library can add the visceral fat in the developed hybrid phantoms according to subject-specific BMI and body fat percentage to construct a more personalized computational phantom.

For internal dosimetry calculations, the differences in mean absorbed doses between the standard model and patient-specific model were about 140% when realistic patient size, habitus and cumulated activity values were considered. (Divoli *et al* 2009) The paediatric phantom library developed in this work is representative of a large number of children habitus and a broad age range of paediatric population. Another related study is being conducted to investigate the effects of body habitus on Monte Carlo-based internal radiation dosimetry calculations using the constructed anthropometric models to quantify the range of errors in patient-specific dose assessment.

5. Conclusion

In this work, we present a methodology for the construction of computational phantoms based on target anthropometric parameters of the paediatric population and constructed a large phantom library with computational models covering the 10th, 25th, 50th, 75th and 90th percentiles of body mass, height, length, BMI and SSR of the newborn, 1, 2, 5, 10 and 15 years-old female and male paediatric population. Hybrid phantoms represent an efficient and flexible way to describe realistically the anatomy of the human body and offer unique advantages for patient-specific modelling in biomedical research. The developed automatic deformation technique can also be used to derive new subject-specific computational phantom libraries at different age groups with specific anthropometry characteristics.

To the best of our knowledge, the newly generated paediatric phantom library is the largest one available today. It offers unique advantages for a wide variety of applications including

imaging physics research and radiation dosimetry, where body size and habitus may have a large influence on image quality and quantitative accuracy as well as patient dose. It can also be used for quick patient-specific absorbed dose assessment in radiation protection and to estimate individual risks in a variety of diagnostic radiology and nuclear medicine examinations.

Acknowledgments

This work was supported by the Swiss National Science Foundation under grant SNSF 31003A-149957 and the Swiss Cancer Research Foundation under Grant KFS-3855-02-2016.

References

Ben Azouz Z, Rioux M, Shu C and Lepage R 2006 Characterizing human shape variation using 3D anthropometric data *Vis. Comput.* **22** 302–14

Bond J *et al* 2012 Series of 4D adult XCAT phantoms for imaging research and dosimetry *Proc. SPIE 8313, Medical Imaging 2012: Physics of Medical Imaging (San Diago, CA)* p 83130P

Caballero B 2007 The global epidemic of obesity: an overview *Epidemiol. Rev.* **29** 1–5

Cassola V, de Melo Lima V, Kramer R and Khoury H 2009 FASH and MASH: female and male adult human phantoms based on polygon mesh surfaces: I. Development of the anatomy *Phys. Med. Biol.* **55** 133–62

Cassola V F, Milian F M, Kramer R, de Oliveira Lira C A and Khoury H J 2011 Standing adult human phantoms based on 10th, 50th and 90th mass and height percentiles of male and female Caucasian populations *Phys. Med. Biol.* **56** 3749–72

Cherubini E, Chavannes N and Kuster N 2009 Realistic skeleton based deformation of high-resolution anatomical human models for electromagnetic simulations *The 31st Annual Meeting of the Bioelectromagnetic Society* (*Ishikawa, Japan*) pp 505–7 (www.ursi.org/proceedings/procGA08/papers/KP1p12.pdf)

Clark L D, Stabin M G, Fernald M J and Brill A B 2010 Changes in radiation dose with variations in human anatomy: moderately and severely obese adults *J. Nucl. Med.* **51** 929–32

Coppoletta J M and Wolbach S B 1933 Body length and organ weights of infants and children: a study of the body length and normal weights of the more important vital organs of the body between birth and twelve years of age *Am. J. Pathol.* **9** 55–70 (PMID: 19970058)

de la Grandmaison G L, Clairand I and Durigon M 2001 Organ weight in 684 adult autopsies: new tables for a Caucasoid population *Forensic Sci. Int.* **119** 149–54

Denecke K and Spreckelsen C 2013 Personalized medicine and the need for decision support systems *Stud. Health Technol. Inform.* **186** 41–5 (PMID: 23542964)

Divoli A *et al* 2009 Effect of patient morphology on dosimetric calculations for internal irradiation as assessed by comparisons of Monte Carlo versus conventional methodologies *J. Nucl. Med.* **50** 316–23

Frisancho A R 2008 *Anthropometric Standards: an Interactive Nutritional Reference of Body Size and Body Composition for Children and Adults* (Ann Arbor, MI: University of Michigan Press)

Gosselin M-C *et al* 2014 Development of a new generation of high-resolution anatomical models for medical device evaluation: the virtual population 3.0 *Phys. Med. Biol.* **59** 5287–303

Hendee W R and O'Connor M K 2012 Radiation risks of medical imaging: separating fact from fantasy *Radiology* **264** 312–21

ICRP 2002 Publication 89: basic anatomical and physiological data for use in radiological protection: reference values *Ann. ICRP* **32** 1–277

Johnson P B *et al* 2009 Hybrid patient-dependent phantoms covering statistical distributions of body morphometry in the US adult and pediatric population *Proc. IEEE* **97** 2060–75

Lee C *et al* 2009 The UF family of reference hybrid phantoms for computational radiation dosimetry *Phys. Med. Biol.* **55** 339–63

Marine P M, Stabin M G, Fernald M J and Brill A B 2010 Changes in radiation dose with variations in human anatomy: larger and smaller normal-stature adults *J. Nucl. Med.* **51** 806–11

McDowell M A, Fryar C D, Ogden C L and Flegal K M 2008 Anthropometric reference data for children and adults: United States, 2003–2006 *Natl Health Stat. Rep.* **10** 1–44 (PMID: 25585443)

Molina D K and DiMaio V J 2015 Normal organ weights in women: part II—the brain, lungs, liver, spleen, and kidneys *Am. J. Forensic Med. Pathol.* **36** 182–7

Na Y H, Zhang B, Zhang J, Caracappa P F and Xu X G 2010 Deformable adult human phantoms for radiation protection dosimetry: anthropometric data representing size distributions of adult worker populations and software algorithms *Phys. Med. Biol.* **55** 3789–811

Neufeld E, Szczerba D, Bühlmann B, Zefferer M and Kuster N 2011 Fast interpolation based morphing of whole body human models *General Assembly and Scientific Symp., 2011 XXXth URSI* pp 1–3

Robbins E 2008 Radiation risks from imaging studies in children with cancer *Pediatr. Blood Cancer* **51** 453–7

Robinette K M, Daanen H and Paquet E 1999 The CAESAR project: a 3D surface anthropometry survey *Proc. of the Second Int. Conf. on 3D Digital Imaging and Modeling* pp 380–6

Sarrut D *et al* 2014 A review of the use and potential of the GATE Monte Carlo simulation code for radiation therapy and dosimetry applications *Med. Phys.* **41** 064301

Schauer D A 2011 Does security screening with backscatter x-rays do more good than harm? *Radiology* **259** 12–6

Schauer D A and Linton O W 2009 NCRP Report No. 160, Ionizing radiation exposure of the population of the United States, medical exposure—are we doing less with more, and is there a role for health physicists? *Health Phys.* **97** 1–5

Segars W P *et al* 2013 Population of anatomically variable 4D XCAT adult phantoms for imaging research and optimization *Med. Phys.* **40** 043701–11

Sheikhazadi A, Sadr S S, Ghadyani M H, Taheri S K, Manouchehri A A, Nazparvar B, Mehrpour O and Ghorbani M 2010 Study of the normal internal organ weights in Tehran's population *J. Forensic Leg Med.* **17** 78–83

Stabin M G *et al* 2012 RADAR reference adult, pediatric, and pregnant female phantom series for internal and external dosimetry *J. Nucl. Med.* **53** 1807–13

Steinert M *et al* 2003 Delayed effects of accidental cutaneous radiation exposure: fifteen years of follow-up after the Chernobyl accident *J. Am. Acad. Dermatol.* **49** 417–23

Thornton R H *et al* 2015 Patient perspectives and preferences for communication of medical imaging risks in a cancer care setting *Radiology* **275** 545–52

Zaidi H 1999 Relevance of accurate Monte Carlo modeling in nuclear medical imaging *Med. Phys.* **26** 574–608

Zaidi H and Xu X G 2007 Computational anthropomorphic models of the human anatomy: the path to realistic Monte Carlo modeling in medical imaging *Annu. Rev. Biomed. Eng.* **9** 471–500